Supporting Information

How Charge Separation and Photoactivity Are Enhanced in Heterostructured g-C_3N_4: A Synergistic Interaction in Environmental Friendly CaO/g-C_3N_4

P.V.R.K. Ramacharyulu, Sk Jahir Abbas, and Shyue-Chu Ke*

Physics Department, National Dong Hwa University, Hualien, Taiwan 97401

Sample characterization: Powder X-ray diffraction patterns were measured on a Bruker D8 Advance diffractometer equipped with a scintillation counter detector with Cu K_α radiation (λ = 0.15418 nm). Diffuse reflectance spectra of powders were measured on a Shimadzu (UV-2550) equipped with an integrating sphere by using $BaSO_4$ as internal standard. The absorption spectra of MB solutions were recorded on a Shimadzu (UV-2550) UV-vis spectrophotometer. X-ray photoelectron spectroscopy (XPS) (Thermo Scientific) measurements was performed with monochromatic Al K_α excitation and a charge neutralizer. Photoluminescence spectra were recorded on a LS 45 Fluorescence Spectrometer of Perkin Elmer. BET measurements were recorded on ASAP 2020 Micrometrics. EPR measurements were performed using a Bruker EMX spectrometer equipped with a TE_{102} cavity for X-band and a ER5106QT cavity for Q-band. A Newport xenon lamp equipped with IR filter and visible filter ($\lambda \geq 420$ nm) was used as the excitation source. All g-C_3N_4 and CaO/g-C_3N_4 samples were irradiated and measured under the same conditions. The g factor was calibrated by reference to a DPPH sample.

Photocatalytic experiments: The photocatalytic activities were evaluated by the decomposition of MB under visible light irradiation. An aqueous solution of MB (100 mL, 10 mg/L) was placed in a vessel, and 20 mg photocatalyst was added. At certain time intervals, 3 mL aliquots were sampled and centrifuged to remove the particles. The filtrates were analyzed by recording variations of the maximum absorption peak.

Supporting Table S1. Fitting Parameters for the Time Dependent Decay of g-C_3N_4 and CaO/g-C_3N_4 Trapped Electron EPR Signal Intensities

	y_0	C_1	k_1 (min^{-1})	C_2	k_2 (min^{-1})
g-C_3N_4	0.15	0.26	2.6	0.36	0.13
CaO/g-C_3N_4					
1:10	0.35	0.23	2.4	0.29	0.18
1:5	0.35	0.21	2.5	0.27	0.21
1:3	0.38	0.16	2.2	0.31	0.17

Supporting Figures:

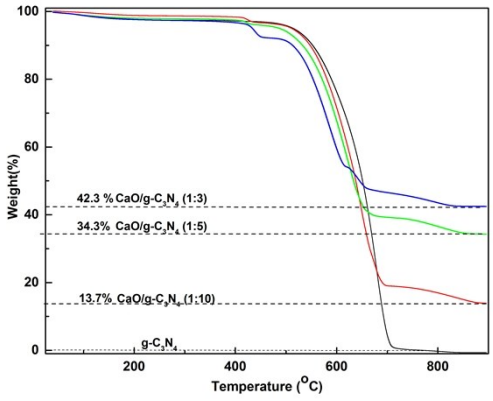

Figure S1A Thermo gravimetric analysis of g-C_3N_4 and CaO/g-C_3N_4 (1:3), CaO/g-C_3N_4 (1:5), CaO/g-C_3N_4 (1:10) composites. TGA was performed to know the exact amount of CaO in CaO/g-

C_3N_4 composites from room temperature to 900°C under air conditions. Pure g-C_3N_4 exhibited a rapid weight loss from 550°C to 700°C which could be ascribed to the complete decomposition of g-C_3N_4. The decomposition temperature was slightly reduced in the CaO/g-C_3N_4 composites. CaO content in the composites could be easily estimated from the weight remain after heating the samples over 700°C and was found to be 42.3%, 34.3% and 13.7% respectively.

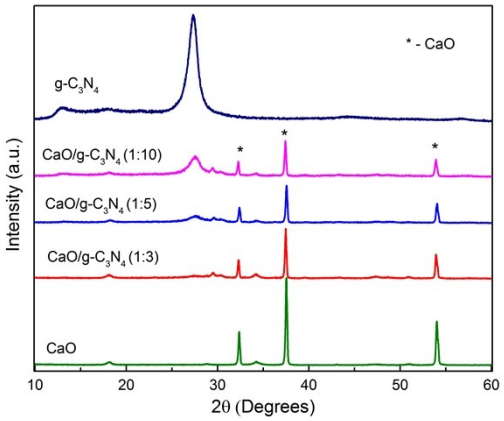

Figure S1B XRD patterns of CaO, CaO/g-C_3N_4 (1:3), CaO/g-C_3N_4 (1:5), CaO/g-C_3N_4 (1:10) and g-C_3N_4. The weak diffraction peak observed at 2θ angles 12.8° corresponds to (1 0 0) plane which represents an in-plane structural packing of g-C_3N_4. The strong diffraction peak at 27.4° corresponds to (0 0 2) plane which depicts the interlayer stacking of conjugated aromatic systems of graphene related materials (g-C_3N_4) which is in consistent with the literature (JCPDS card 87-1526). As for CaO/g-C_3N_4 composites the characteristic diffraction peaks of g-C_3N_4 were observed in addition to CaO peaks. Peaks at 32.36°, 37.5° and 54.0° corresponds to (111), (200) and (220) planes of CaO.

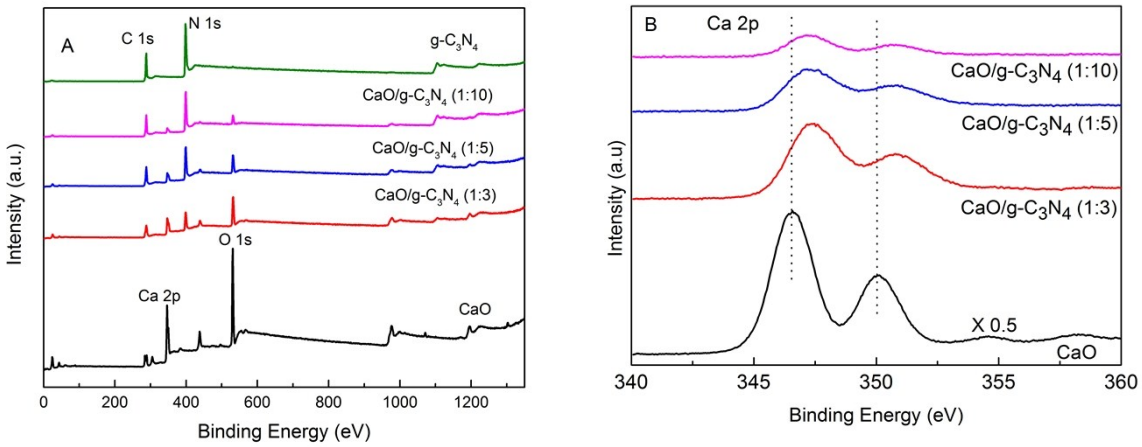

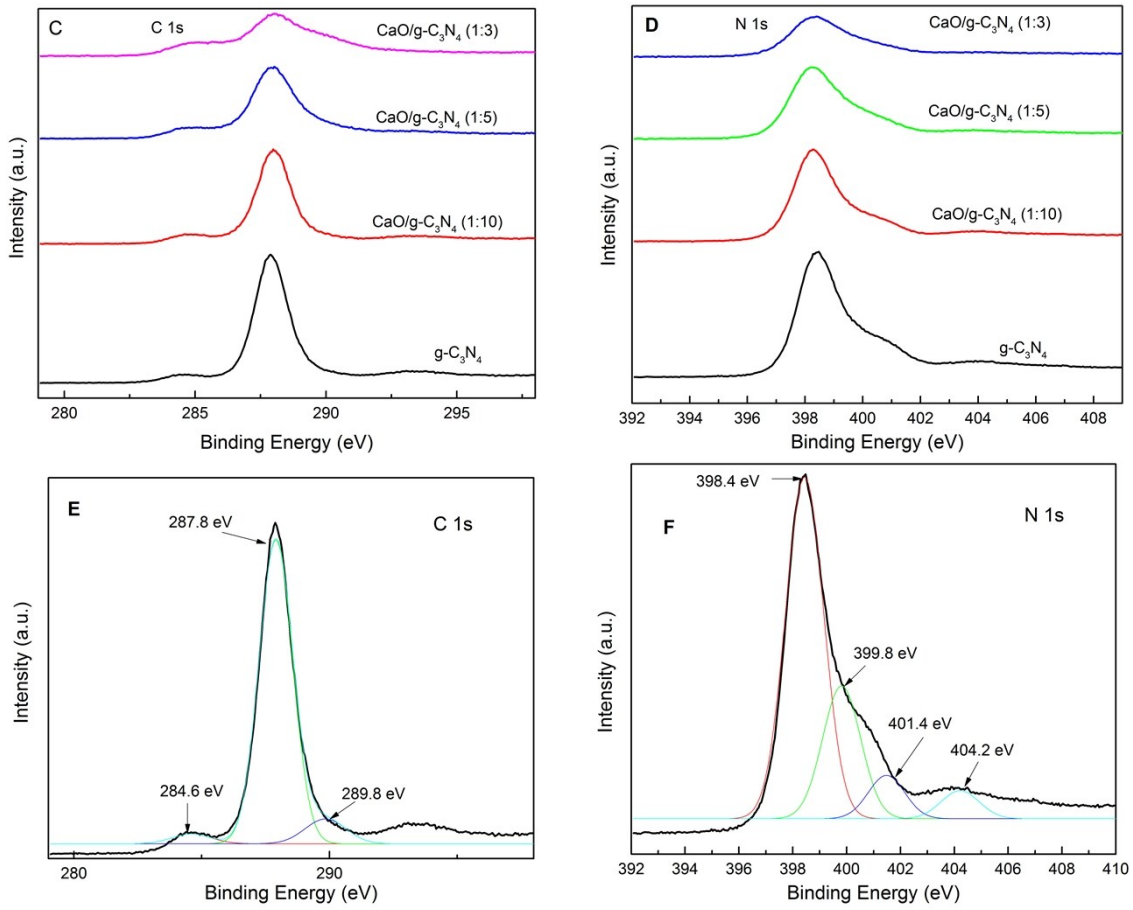

Figure S2. The peaks located at 287.8, 399.5, 530.7, 346.3 and 349.8 eV are assigned to C 1s, N 1s, O1s and Ca 2p respectively. N 1s of g-C_3N_4 is deconvoluted into four peaks at 398.4, 399.8, 401.4 and 404.2 eV which can be assigned to sp^2 hybridized N in C−N=C, N−$(C)_3$, incomplete condensation in C−N−H and π excitation respectively. C 1s spectrum is deconvoluted into three components at about 284.6, 287.8, and 289.8 eV. The peaks centered at 284.6, 287.8 eV are ascribed to sp^2 C atoms bonded to N in an aromatic ring (N−C=N), C−$(N)_3$ and the peak situating at 287.8 eV can be assigned to the pure graphitic sites in a C−N−C coordination.[1]

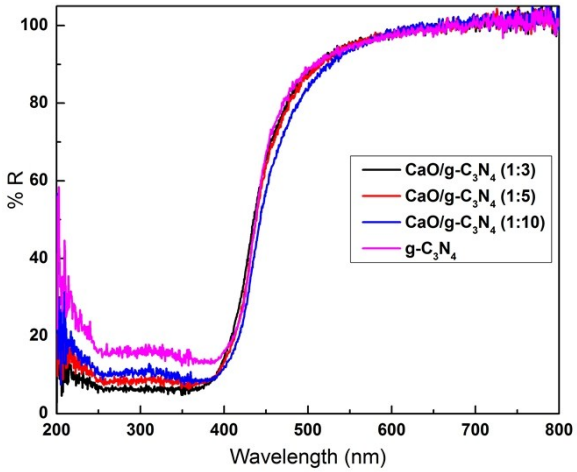

Figure S3 Diffuse reflectance spectra of CaO/g-C_3N_4 (1:3), CaO/g-C_3N_4 (1:5), CaO/g-C_3N_4 (1:10) and g-C_3N_4.

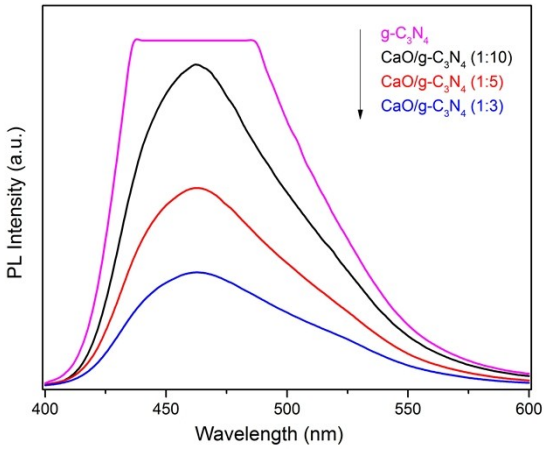

Figure S4. Photoluminescence (PL) spectra of CaO/g-C_3N_4 (1:3), CaO/g-C_3N_4 (1:5), CaO/g-C_3N_4 (1:10) and g-C_3N_4. Emission spectra were recorded under the excitation wavelength of 320 nm. PL measures the radiative recombination of photogenerated excitons. The higher degree of PL quenching has been widely used as an indicator for slower charge recombination rate leading to higher photocatalytic activity. And, the slow recombination rate is often further implicated as a result of charge transfer across interfaces. However, Figure S4 shows that the PL intensity in the following descending order: g-C_3N_4 > 1:10 > 1:5 > 1:3 CaO/g-C_3N_4 does not follow the activity trend (Figure 1). We note that the PL intensity also reflects the amount of C_3N_4 in the mixture. The degree of structural imperfection could also induce non-radiative recombination. Therefore, we suggest that PL intensity should not be used as a hallmark feature for implicating the mechanism for enhanced charge carrier separation efficiency.

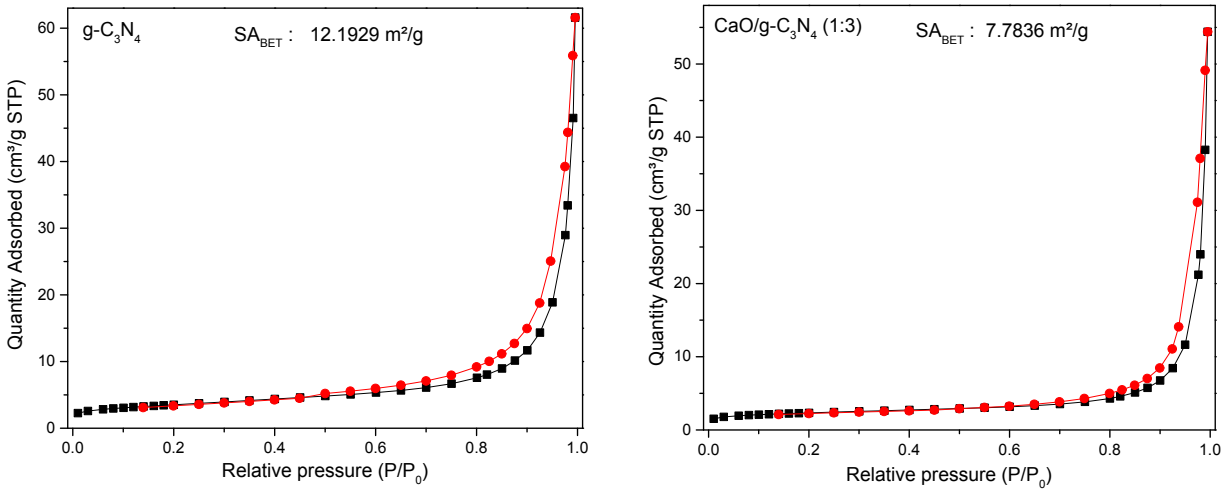

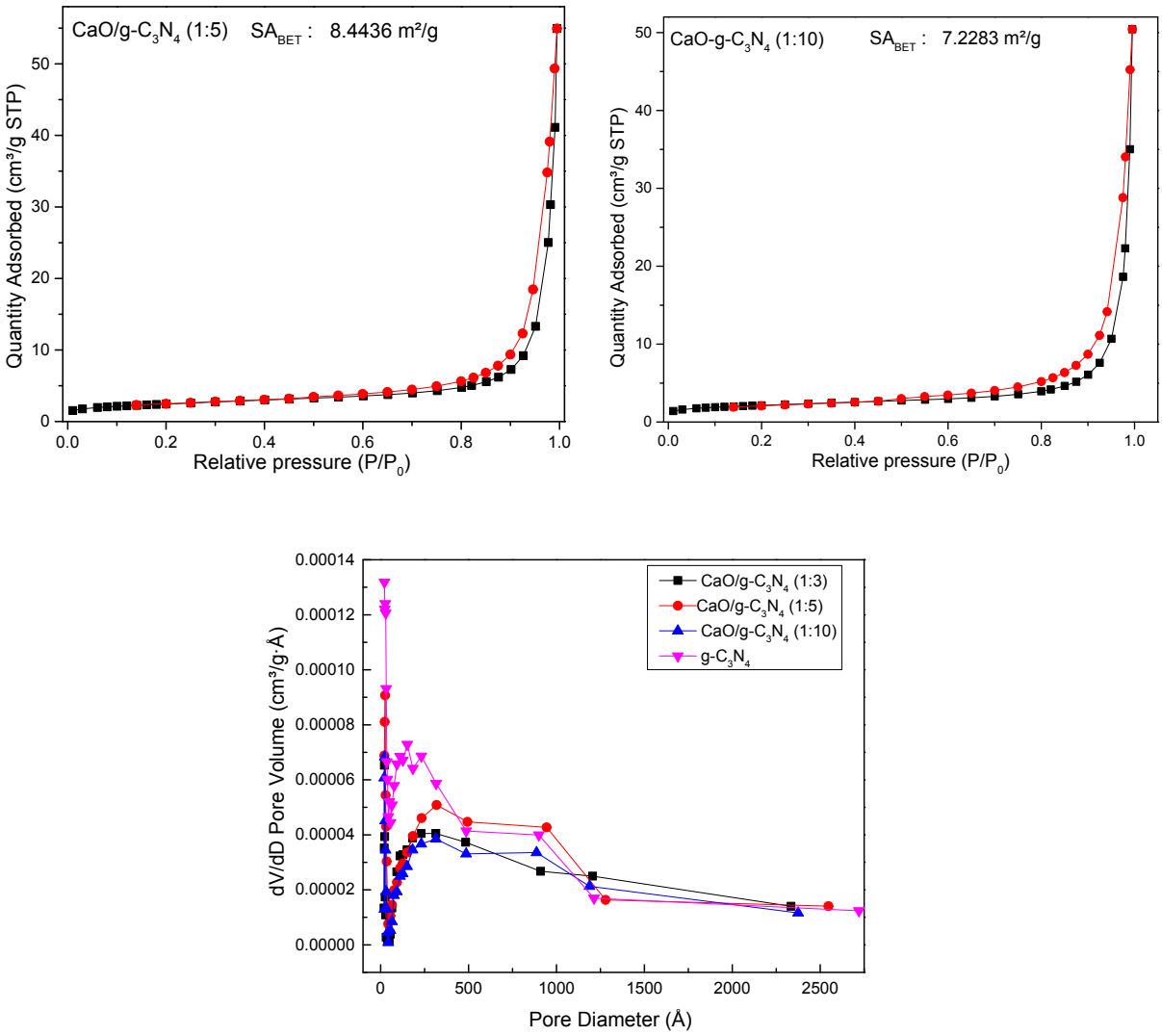

Figure S5. Nitrogen adsorption-desorption isotherms and pore size distribution of g-C_3N_4 and CaO/g-C_3N_4 (1:3), CaO/g-C_3N_4 (1:5) and CaO/g-C_3N_4 (1:10) composites.

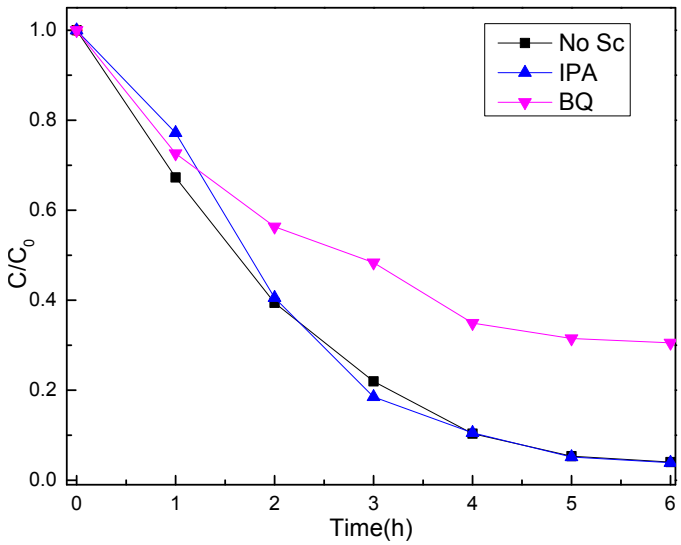

Figure S6A. Radical quenching measurements of 1:5 CaO/g-C_3N_4. Addition of $O_2^{-\bullet}$ quencher, benzoquinone, reduces the activities by ~ 60 % whereas the activity is unaffected by the $OH^{\bullet}$

quencher isopropanol. This indicates that the surface O_2 reduced by the C_{2p} electrons is the main reactive species in the reaction.

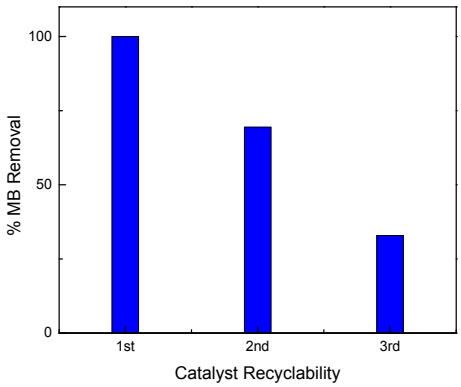

Figure S6B. Photocatalyst stability study of CaO/g-C_3N_4 (1:5). After each photocatalytic experiment, the catalyst was centrifuged, washed with dd-H_2O, dried and reused for three consecutive runs which removed 100, 69.5 and 32.9% of MB, respectively.

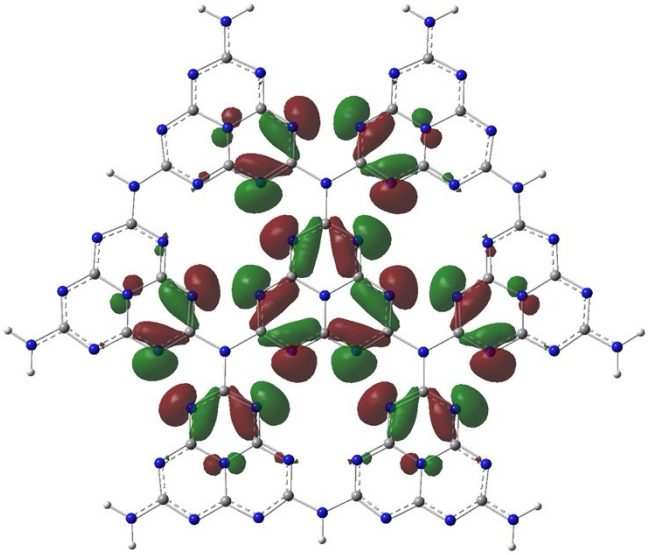

Figure S7**.** The HOMO of planar g-C_3N_4 describing the delocalized nitrogen lone pair orbitals lies on the plane of g-C_3N_4.

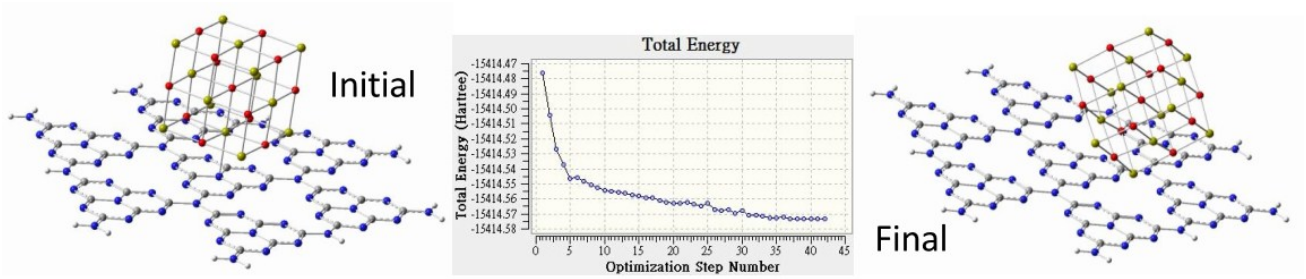

Figure S8**.** Geometry optimizations were performed in gas phase at the B3-LYP level with 6-31G(d,p) basis. The Gaussian 03 suite of programs[2] was used for all calculations.

Optimized XYZ coordinates for CaO/g-C_3N_4 truncated with NH_2:

C	6.05727000	4.05787400	-0.11704300
C	7.84009000	5.59797200	0.47001500
C	8.16465500	3.15768000	0.57708400
C	6.39446200	1.81300500	-0.00582900
C	9.80073700	4.64102900	1.11581800
C	4.41142300	0.30437800	-0.65883100
C	6.66785300	-0.69195100	0.08439000
C	6.82368600	-2.95874500	0.13587400
C	7.04543400	-5.21152000	0.20906700
C	8.89231100	-4.03218600	0.81724700
C	5.15067100	-6.69091000	-0.41486300
C	3.16752500	-5.81341500	-1.06807000
C	3.54255600	-8.20918800	-0.94438400
C	2.69340300	-1.11968600	-1.22478800
C	0.90198600	-2.43570800	-1.81446000
C	2.43205400	1.28055700	-1.31089800
C	0.58962000	-0.15920800	-1.91748600
C	1.15248500	-4.99822600	-1.73177600
C	-1.04496300	-3.99571500	-2.45557200
C	1.37323800	-7.28468500	-1.65890900
C	-2.78107000	-5.38875700	-3.02725500
C	1.77486200	-9.51808700	-1.52647600
C	8.68189500	-1.57819600	0.74777300
C	-2.98736400	-3.00419900	-3.09536800
C	10.59523000	-2.63128400	1.37800000
N	11.86824600	-2.51251200	1.79725600
N	10.14425300	-3.89806000	1.22956200
N	8.32398800	-5.23110000	0.63015700
N	6.45186900	-6.45350100	0.01366600
N	4.79727100	-7.98473100	-0.53116200
N	3.05717000	-9.43155900	-1.10415800
N	1.29730500	-10.76615300	-1.68367000
N	9.93858000	-1.47150400	1.16165100
N	8.14096200	-2.86117300	0.56970900
N	6.29448600	-4.14987600	-0.03833200
N	4.40381400	-5.62609100	-0.66091500
N	2.69640600	-7.11221500	-1.22313900
N	0.91139700	-8.51981000	-1.81092800
N	7.92370300	-0.51106400	0.49798800

N	6.10503800	-1.87328900	-0.10088800
N	2.38964300	-4.77421500	-1.32433700
N	0.62349200	-6.21100300	-1.90591300
N	11.06609500	4.82986300	1.53254700
N	9.41150900	3.35445100	0.98771800
N	7.65652600	1.93711100	0.40982000
N	5.82763100	0.47551800	-0.19241800
N	3.94930600	-0.93816200	-0.81096500
N	2.16557900	-2.33089200	-1.39834300
N	0.33534900	-3.81288200	-2.00098200
N	-1.52414000	-5.23120700	-2.61330000
N	-3.32192800	-6.58782100	-3.20530000
C	-4.60431200	-6.60643800	-3.62764900
C	-4.90478800	-4.35323000	-3.72677000
N	-5.14332900	-7.82645500	-3.80508600
N	9.08821600	5.76682600	0.88107000
N	7.36114800	4.27783800	0.31237100
N	5.59164600	2.82892400	-0.27030700
N	3.69340300	1.40418700	-0.89526500
N	1.90611200	0.00279200	-1.48352200
N	0.11088400	-1.39307500	-2.07504000
N	-1.73518300	-2.89193100	-2.68297300
N	-3.56585300	-4.25401100	-3.28580300
N	-5.42063900	-5.56169900	-3.89657900
C	5.78709600	6.30471300	-0.20618300
C	0.40262400	2.13450100	-1.97924900
C	-3.50798100	1.75766000	-3.26717000
C	-1.83022100	3.18783800	-2.71470600
C	0.09344300	4.68997700	-2.08125900
C	1.88044000	5.96502200	-1.49280700
C	3.62295500	7.29295300	-0.91900800
C	1.72988400	8.38779800	-1.54256500
C	-0.18405900	6.96960500	-2.17281600
C	-3.82160300	4.12928700	-3.37063000
C	-0.27363000	9.24074900	-2.20247800
N	5.28479600	5.09122400	-0.37152900
N	7.02799200	6.62959300	0.20247900
N	1.65586400	2.33445100	-1.56664100
N	-0.14299300	0.92990000	-2.15892500
N	-3.70226200	-1.92593200	-3.33089400
N	-0.44660700	3.34005200	-2.25902700
N	-2.26430900	1.94775200	-2.85758400
N	-3.97160800	0.53659100	-3.41977800
N	1.34654800	4.76723100	-1.66855700
N	3.12484100	6.07758300	-1.08297500
N	4.94131400	7.37244200	-0.48481600
N	3.00022800	8.46868500	-1.12418600
N	1.14177000	7.11745200	-1.73616800
N	-0.68303500	5.74482700	-2.33706500
N	-2.56357000	4.27638400	-2.95631000
N	-4.34094600	2.83643300	-3.54158200
N	-4.60697100	5.16764700	-3.62936300
N	-0.89979000	8.06233700	-2.40861800
N	0.99394000	9.46247300	-1.78502200

C	-4.95104800	-2.07964200	-3.74216800
N	-5.60659500	-3.23552400	-3.95798900
N	-5.67590300	-0.91754100	-3.98098000
C	-5.22085900	0.38764800	-3.83120500
C	-5.66629600	2.61277200	-3.97806700
N	-6.10868300	1.35638600	-4.12367700
N	-1.00729100	10.34244600	-2.44418600
C	-5.85980000	4.87892200	-4.04195900
N	-6.42938000	3.66623700	-4.22946200
N	-6.64810900	5.93794300	-4.30166200
H	11.41260900	5.76783800	1.64660300
H	11.64377800	4.02801200	1.72286200
H	12.25789700	-1.59347600	1.92552100
H	12.40804500	-3.34309800	1.97509700
H	5.32359100	8.30044200	-0.35898000
H	7.02414000	-7.26596100	0.20220000
H	0.34886500	-10.89186400	-1.99602700
H	1.89549800	-11.55114200	-1.48660000
H	-0.59355600	11.24973000	-2.30798800
H	-1.95812800	10.23872200	-2.75733400
H	-6.27774600	6.86578000	-4.17974900
H	-7.59285400	5.78451800	-4.61280000
H	-6.63034800	-1.03322500	-4.29531600
H	-6.09645500	-7.90324300	-4.11899000
H	-4.58227900	-8.64129200	-3.62024700
O	-3.17794800	1.62342500	-0.18465400
O	-6.63625300	-0.76895900	1.94369600
O	-5.62170300	2.44141300	1.87211400
O	-4.16952300	-1.62761600	-0.15497900
O	-4.46287400	-3.20073600	2.77094700
O	-0.94260400	-0.82489700	0.63752200
O	-0.26447900	0.76539400	3.47101300
O	-3.76541800	-1.59809400	5.63498600
O	-1.28817800	-2.43878000	3.53473500
O	-2.74794600	1.60099800	5.56240800
O	-2.42808400	3.20149000	2.63852900
O	-5.92550500	0.83213100	4.80374200
O	-3.45455400	-0.00343700	2.71310600
Ca	-5.25030500	-1.22494900	3.81533100
Ca	-7.24408900	1.21240700	2.93995600
Ca	-4.20489900	2.08099100	3.73457300
Ca	-1.97151900	-0.43109100	4.59579900
Ca	-4.46201800	0.40822000	6.53431700
Ca	-1.06376500	2.69968800	4.41905800
Ca	-3.84769400	3.53445000	0.84807900
Ca	-1.64071200	1.20892500	1.54507500
Ca	0.36225100	-1.22655300	2.46892600
Ca	-4.90360500	0.41423600	0.76549000
Ca	-2.67691500	-2.06976200	1.59502600
Ca	-5.83158700	-2.70554800	0.97659600
Ca	-2.39134400	-0.41996700	-1.38571300
Ca	-3.04221200	-3.50886300	4.54895300

References:

(1) Shi, L.; Liang, L.; Ma, J.; Wang, F.; Sun, J. Catal. Sci. Technol., 2014, 4, 758.
(2) Gaussian 03, Revision C.02, Frisch, M. J.; Trucks, G. W.; Schlegel, H. B.; Scuseria, G. E.; Robb, M. A.; Cheeseman, J. R.; Montgomery Jr, J. A.; Vreven, T.; Kudin, K. N.; Burant, J. C.; Millam, J. M.; Iyengar, S. S.; Tomasi, J.; Barone, V.; Mennucci, B.; Cossi, M.; Scalmani, G. Rega, N.; Petersson, G. A.; Nakatsuji, H.; Hada, M.; Ehara, M.; Toyota, K.; Fukuda, R.; Hasegawa, J.; Ishida, M.; Nakajima, T.; Honda, Y.; Kitao, O.; Nakai, H.; Klene, M.; Li, X.; Knox, J. E.; Hratchian, H. P.; Cross, J. B.; Bakken, V.; Adamo, C.; Jaramillo, J.; Gomperts, R.; Stratmann, R. E.; Yazyev, O.; Austin, A. J.; Cammi, R.; Pomelli, C.; Ochterski, J. W.; Ayala, P. Y.; Morokuma, K.; Voth, G. A.; Salvador, P.; Dannenberg, J. J.; Zakrzewski, V. G.; Dapprich, S.; Daniels, A. D.; Strain, M. C.; Farkas, Ö.; Malick, D. K.; Rabuck, A. D.; Raghavachari, K.; Foresman, J. B.; Ortiz, J. V.; Cui, Q.; Baboul, A. G.; Clifford, S.; Cioslowski, J.; Stefanov, B. B.; Liu, G.; Liashenko, A.; Piskorz, P.; Komaromi, I.; Martin, R.L.; Fox, D. J.; Keith, T.; Al–Laham M. A.; Peng, C. Y.; Nanayakkara A.; Challacombe, M.; Gill, P. M. W.; Johnson, B.; Chen, W.; Wong, M. W.; Gonzalez, C.; Pople, J. A. Gaussian, Inc., Wallingford CT, 2004.